Analysis of Oriented Textures using Mathematical Morphology

Allan Hanbury[1)]
Pattern Recognition and Image Processing Group, Vienna University of Technology,
Favoritenstraße 9/1832, A-1040 Wien, Austria. E-mail: hanbury@prip.tuwien.ac.at

Jean Serra
Centre de Morphologie Mathématique, Ecole des Mines de Paris,
35 rue Saint-Honoré, 77305 Fontainebleau cedex, France

Abstract:
Oriented textures are characterised by a dominant orientation at each point of the texture, and can be summarised by images encoding these dominant orientations. Because of the angular values in these images, standard morphological operators are not suited to their treatment. We discuss the application of the morphological circular centred operators to the analysis of oriented textures for the specific case of wood texture. The circular centred gradient is applied to the segmentation of oriented textures, and the circular centred top-hat to the detection of defects in these textures.

1 Introduction

Four classes of texture have been defined by Rao [13]: strongly ordered texture, weakly ordered texture, disordered texture and compositional texture. In this paper we consider the second type, weakly ordered texture. This type of texture is characterised by a high level of orientation specificity at each point of the texture, and is also referred to as *oriented texture*. The veins on a plank of wood are a good example of this type of texture.

A convenient representation for the analysis of oriented texture is a two-dimensional vector field. Each vector is associated with a point in the texture: the vector's direction represents the orientation at that point; and its length is a measure of the orientation "strength" or "coherence". The vector field can be encoded by two greyscale images, an *orientation image*, in which the direction of each vector is represented by the pixel values, and a corresponding vector "strength" image.

In section 2, we describe an algorithm for calculating the orientation image of an oriented texture. Section 3 presents the circular centred morphological operators, which are applied to texture seg-

[1)] Part of this work was done while the author was with the Centre de Morphologie Mathématique, Ecole des Mines de Paris, France. It is supported by the Austrian Science Foundation (FWF) under grants P14445-MAT and P14662-INF.

mentation in section 4, and to defect detection in section 5. The example images used are taken from a study performed for an industrial partner (Scanwood System, Pont-à-Mousson, France) working in the field of automated wood inspection, but the algorithms can certainly be applied to other oriented textures.

2 Calculating the orientation image

Several algorithms exist for calculating the descriptive vector fields of oriented textures. We use an algorithm suggested by Rao and Schunck [13], of which a brief description is given here:

1. The original greyscale image is smoothed by a Gaussian filter with standard deviation σ_1 to choose the scale that will be analysed.

2. For each pixel (k, l), the horizontal and vertical gradients H_{kl} and V_{kl} are calculated, and from these, the modulus R_{kl} and the angle θ_{kl} ($0^\circ \leq \theta_{kl} \leq 360^\circ$) are calculated.

3. A neighbourhood W with width σ_{2h} and height σ_{2v} is moved over the image in steps of size Δ_h pixels horizontally and Δ_v pixels vertically. At each position (x, y) of the neighbourhood, the dominant local orientation $\widehat{\theta}_{xy}$ ($0^\circ \leq \widehat{\theta}_{xy} \leq 180^\circ$) is calculated:

$$\widehat{\theta}_{xy} = \frac{1}{2} \arctan \frac{\sum_{(k,l)\in W} R_{kl}^2 \sin 2\theta_{kl}}{\sum_{(k,l)\in W} R_{kl}^2 \cos 2\theta_{kl}} \tag{1}$$

   An orientation of 90° indicates vertical structures, and orientations of 0° and 180° indicate horizontal structures. Notice that the veins are undirected lines, which explains the 180° periodicity of the calculated orientations.

4. An orientation summary image $\overline{\theta}$, which encodes the distribution of the orientations, is built. In this image, the value of each pixel represents the dominant orientation calculated in a neighbourhood. Symbolically, $\overline{\theta}_{kl} = \widehat{\theta}_{(k\times\Delta_h)(l\times\Delta_v)}$.

The above algorithm has a number of parameters to set, and their values depend on the application for which the orientation image is to be used. The first is σ_1, which controls the scale of the texture to be analysed. The value of this parameter can significantly change the results of the algorithm if the texture contains differently oriented structures at different scales (for example, thick and thin lines with different orientations).

The size ($\sigma_{2h} \times \sigma_{2v}$) of the neighbourhood W is less critical. It should be large enough to always overlap one "oriented structure" at each position. If the orientation image is used to find defects which are characterised by anomalous orientations, then the neighbourhood should be smaller or equal in size to the defects to be detected. This avoids blurring the defect orientations with the surrounding orientations. The step sizes Δ_h and Δ_v of the neighbourhood can be adjusted to give

an orientation image of the required size, however, if all the pixels in the initial greyscale image are to be taken into account, then it is necessary that $\Delta_h \leq \sigma_{2h}$ and $\Delta_v \leq \sigma_{2v}$.

The Rao and Schunck algorithm is a fast and simple method for calculating the dominant orientations of a texture. A multi-scale description of an oriented texture can easily be calculated by replacing steps 1 and 2 of the algorithm by a Dyadic Wavelet transform [11]. Davies [5] suggests some convolution kernels that could increase the accuracy of the orientation detection of linear structures (in step 2). The main drawback of the Rao and Schunck algorithm is its inability to calculate more than one dominant orientation in a neighbourhood. An algorithm capable of detecting two dominant orientations is presented by Andersson and Knutsson [1]. For the detection of multiple orientations, Chetverikov [3] uses a measure of anisotropy, and Freeman and Adelson [7] use steerable filters, a generalisation of filter banks.

3 Mathematical morphology and circular data

Circular data consist of values measured as angles (i.e. in units of degrees or radians). The application of mathematical morphology to circular data is difficult, as there is no obvious origin, and because the data is periodic. Some rotationally invariant morphological operators, which do not require the choice of an origin, are introduced in [8, 9]. The circular centred operators used in this paper are of this type.

The difference between two angular values a_i and a_j is taken to be the smallest angle (acute angle) between them. For the texture images treated in this paper, which have 180° periodicity, this difference is written as

$$a_i \div a_j = \begin{cases} |a_i - a_j| & \text{if} \quad |a_i - a_j| \leq 90^\circ \\ 180^\circ - |a_i - a_j| & \text{if} \quad |a_i - a_j| \geq 90^\circ \end{cases} \tag{2}$$

The circular centred morphological gradient and top-hat operators are derived by rewriting their standard morphological versions in a form which takes into account only *differences* between pixel values, and then replacing these differences by the angular differences of equation 2 [9]. Note that not all morphological operators can be rewritten in this form.

3.1 Circular centred gradient

The circular centred gradient is based on the standard morphological (Beucher) gradient [14], and is calculated by applying the following to each point x in an image $a(x)$ containing angular values

$$g_a(x) = \vee [a(x) \div a(y), y \in B(x)] - \wedge [a(x) \div a(y), y \in B(x)] \tag{3}$$

where $B(x)$ is a structuring element (SE), and the symbols $\vee$ and $\wedge$ represent the supremum and infimum respectively. For the case where the origin is included in the structuring element (the case

most often encountered in practice), the rightmost part of equation 3 is always zero, so the equation becomes

$$g_a(x) = \vee [a(x) \div a(y), y \in B(x)] \tag{4}$$

3.2 Circular centred top-hat

The morphological top-hat is defined [14] as the difference between the original image and its opening by a structuring element B. This expression can also be rewritten in terms of pixel differences, and hence used on angular valued images [8]. To calculate the circular centred top-hat of an angular valued image $a(x)$, the following expression is evaluated at each point x of $a(x)$

$$\mathrm{ATH}[a(x)] = - \vee \{- \vee [a(x) \div a(y), y \in B_i], i \in I\} \tag{5}$$

where $\{B_i, i \in I\}$ is the family of structuring elements B which contain point x.

4 Segmentation

The watershed algorithm [15] can be applied to the gradient of an orientation image (describing an oriented texture) to segment the texture into regions of homogeneous orientation. The steps in the segmentation algorithm, which are illustrated in figure 1, are:

1. The Rao and Schunck algorithm is applied to the initial image (a plank of oak, figure 1a) to calculate the orientation image (figure 1b). For the example, the parameters $\sigma_1 = 1.4$, $\sigma_{2h} = \sigma_{2v} = 64$ and $\Delta_h = \Delta_v = 8$ were used.

2. The circular centred gradient of the orientation image is calculated (figure 1c). For the example, a 5×5 SE was used.

3. The minima are extracted. For the example, we close the gradient image with a 3×3 SE, and then find the h-minima [15] of height $h = 5$ (figure 1d).

4. The watershed is applied to the gradient image using the minima extracted in the previous step as markers (to avoid over-segmentation). For visualisation purposes, the segmentation obtained is superimposed on the initial image in figure 1e; in which the black lines represent the watershed lines. Each region can be characterised by calculating circular statistics [6] (e.g. the orientation mean and variance) of the pixels included in the region (in figure 1e, the blue channel encodes the mean orientation in each region).

Some further results of the segmentation of oriented textures are shown in figure 2. The aim of this segmentation is attained, with the resultant images showing planks well segmented into regions of homogeneous vein orientation. In general, the planks which have the most homogeneous orientations have the fewest regions. A number of problems are nevertheless present: the first is common to

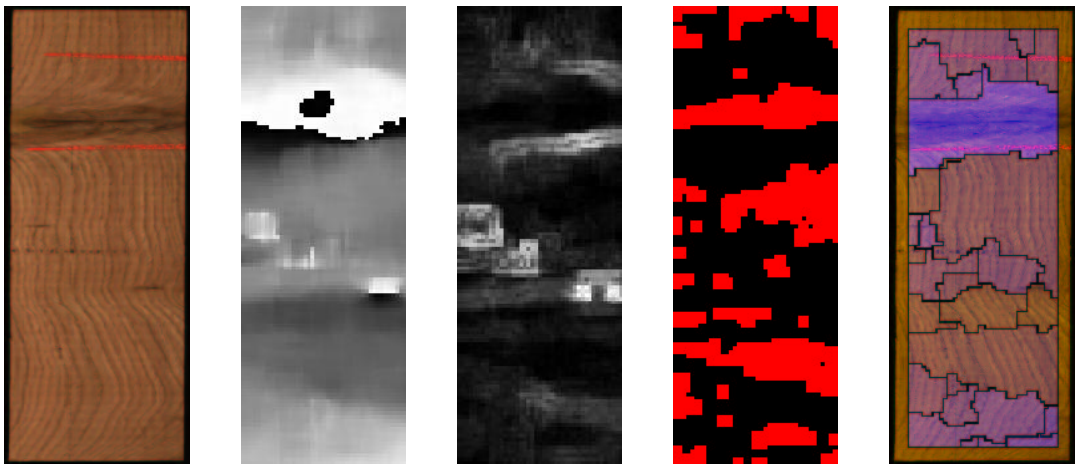

Figure 1: Steps in the segmentation of an oriented texture. (a) Initial image with size 420×1040 pixels (the horizontal red lines visible on the colour image are chalk lines drawn on the board, and are of no importance). (b) Orientation image with size 50×125 pixels. (c) Morphological circular centred gradient (5×5 SE). (d) Minima (watershed markers). (e) Watershed segmentation projected onto the initial image (in the colour image, the blue channel encodes the mean orientation in each region).

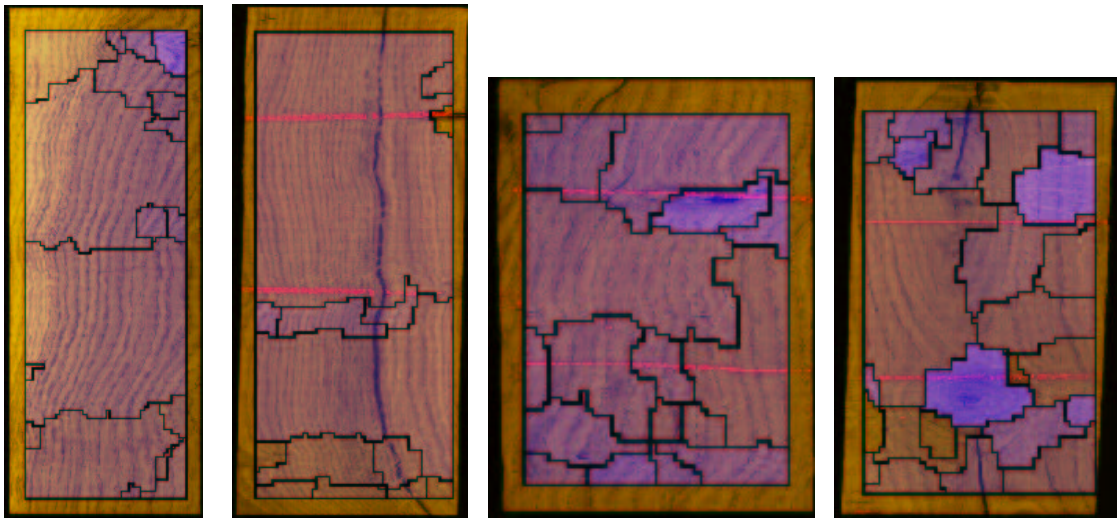

Figure 2: Results of segmentations of oriented textures by the watershed algorithm for four oak images. In the colour images, the blue channel encodes the average orientation in each region.

all watershed segmentations, and involves the choice of markers. If we take all the gradient minima as markers, then an over-segmentation is produced. With the small closing and the use of h-minima, we reduce the number of regions, but a small change in the value of the parameter h can significantly change the resultant partition. For the segmentation of an oriented texture, the partition can also be changed by varying the scale parameter (σ_1) in the calculation of the orientation image. The final problem is seen when the vein orientation varies slowly over too large a region to be detected by the structuring element used to calculate the gradient. This could result in regions that contain several

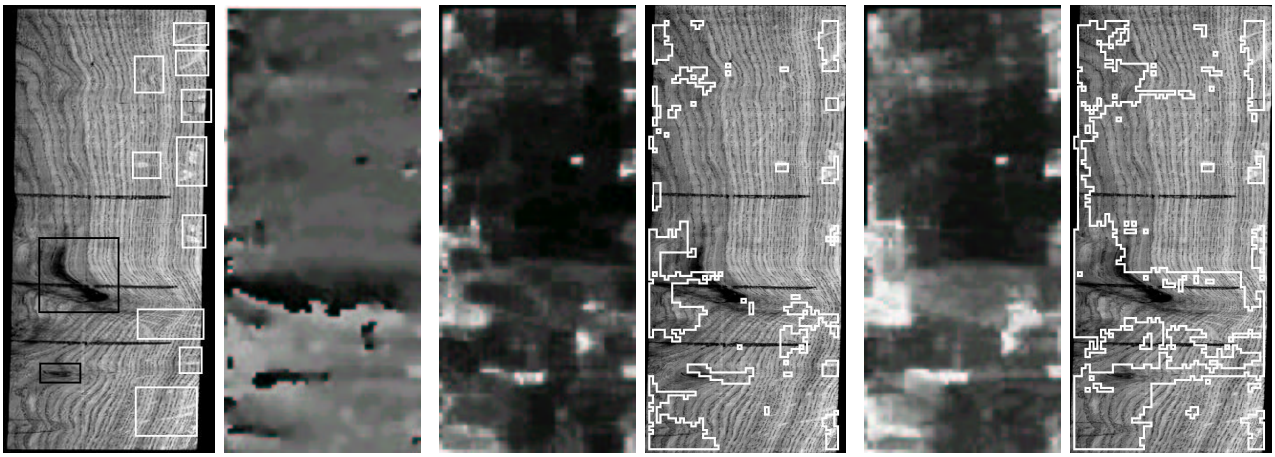

(a) (b) (c) (d) (e) (f)

Figure 3: Defect detection with the morphological circular centred top-hat. (a) Initial image with the defects marked manually (size 608×955 pixels). (b) Orientation image (size 50×112 pixels). (c) Top-hat with 5×5 pixel SE. (d) Threshold on image c projected onto the initial image. (e) Top-hat with 9×9 pixel SE. (f) Threshold on image e projected onto the initial image. For the projected images, the regions inside the white lines correspond to the thresholded regions. The three dark horizontal lines on images a, d and f are chalk marks on the board, and are of no importance.

orientations. Possible solutions to the above problems remain to be studied. One could, for example, start with an over-segmented image, and then fuse regions with similar orientations with the aid of a graph of the partition [10, 12].

5 Defect detection

The morphological circular centred top-hat operator is well suited to finding defects which are characterised by a perturbation in the orientation field. Figure 3 shows an example of defect detection on an oak board. In figure 3a, the two principal defects which perturb the vein orientations are marked manually: knots (marked by black rectangles) and small light patches (marked by white rectangles). The knots are often easily detectable due to their dark colour. However, certain types of knots are not characterised by a change in colour, but only by a perturbation in the directions of the surrounding veins. The light patches have a similar colour to other parts of the wood, but they cause discontinuities in the veins, giving rise to local perturbations in the orientation field. The orientation image (figure 3b) was calculated using the following parameters: $\sigma_1 = 1.4$, $\sigma_{2h} = \sigma_{2v} = 24$ and $\Delta_h = \Delta_v = 8$.

Figures 3c and 3e show the results of a circular centred top-hat operator applied to the orientation image (figure 3b), with a 5×5 pixel structuring element (SE) used for figure 3c, and a 9×9 pixel SE for figure 3e. As expected, this operator highlights the regions which contain large differences in angular values, with the size of the region found being proportional to the size of the SE. Finally, we

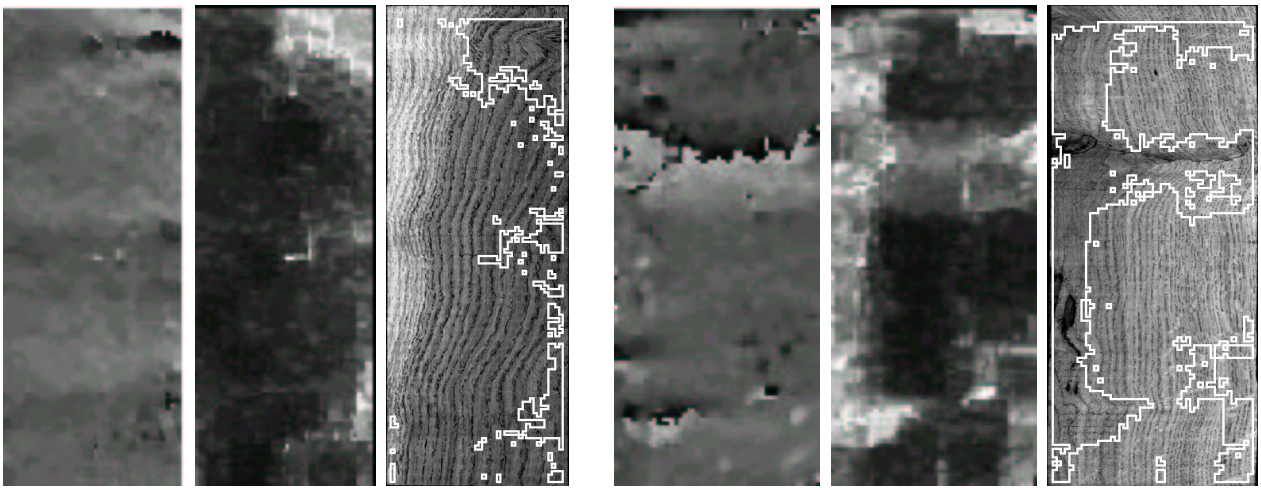

(a) (b) (c) (d) (e) (f)

Figure 4: Two further examples of defect detection with the morphological circular centred top-hat. (a) and (d) Orientation images. (b) and (e) Top-hats with 9×9 pixel SEs. (c) and (f) Thresholds on the top-hat images projected onto the initial images. The regions inside the white lines correspond to the thresholded regions.

threshold the top-hat images to obtain the regions with strong angular variation (for this example, more than $30°$). The thresholded regions, which are shown bounded by white lines, are projected onto the initial image in figures 3d and 3f.

With both sizes of structuring element, the majority of the small light patches are detected. The large knot is not detected with the 5×5 SE, as it is too large with respect to the SE to be considered an anomaly. With the 9×9 SE, the lower part of this knot is detected. The upper part could never be detected using this technique, as it is parallel to the surrounding veins and hence not an orientation anomaly. This operator is not designed to accurately detect the boundaries of the knots, but detects the region around the knot in which the vein orientations are perturbed, as can be seen for the two knots at the bottom of the example image. Nevertheless, vein perturbations are not always associated with defects, as is demonstrated in the upper left area of the example image.

Two further results are shown in figure 4: the orientation image, the top-hat image and the thresholded top-hat projected onto the initial image are shown for each example. Figure 4c shows a board with a fairly constant vein orientation; the small knot at the top right and some vein orientation perturbations on the right are detected. Figure 4f shows a board on which the light patches on the right, the knots on the left and the horizontal linear defect (which is not well marked by a colour difference) are detected.

The use of the top-hat operator does not represent a complete approach to defect detection in the case of wood: not all orientation perturbations are associated with defects, and not all types of defect perturb the orientation. The top-hat image is, however, a valuable component in a defect detection system as it allows the orientation perturbation to be taken into account along with other features

(e.g. colour and texture features) in a statistical decision process. An approximation to this top-hat operator, which has a far shorter calculation time, is described in [9].

6 Conclusion

In this paper, the application of circular centred morphological operators to oriented texture analysis is discussed. We show the use of the circular centred gradient operator in texture segmentation, and the use of the circular centred top-hat operator in defect detection. The examples given here include only uni-directional textures made up of parallel lines. However, the circular centred top-hat operator has been successfully used to detect defects in some anisotropic textures having several principal orientations, of which one is dominant [4]. A comparison of defect detection in some Brodatz textures [2] using the circular centred top-hat and an algorithm based on regularity is given in [4].

References

[1] Mats T. Andersson and Hans Knutsson. Orientation estimation in ambiguous neighbourhoods. In *Proceedings of the Scandinavian Symposium on Image Analysis*, August 1991.

[2] P. Brodatz. *Textures: a photographic album for artists and designers*. Dover, New York, 1966.

[3] Dmitry Chetverikov. Texture analysis using feature-based pairwise interaction maps. *Pattern Recognition*, 32:487–502, 1999.

[4] Dmitry Chetverikov and Allan Hanbury. Finding defects in texture using regularity and local orientation. *Pattern Recognition*, 35(10), September 2002.

[5] E. R. Davies. Vectorial strategy for designing line segment detectors with high orientation accuracy. *Electronics Letters*, 33(21):1775–1777, October 1997.

[6] N. I. Fisher. *Statistical Analysis of Circular Data*. Cambridge University Press, 1993.

[7] William T. Freeman and Edward H. Adelson. The design and use of steerable filters. *IEEE Transactions on Pattern Analysis and Machine Intelligence*, 13(9):891–906, September 1991.

[8] Allan Hanbury. *Morphologie Mathématique sur le Cercle Unité: avec applications aux teintes et aux textures orientées*. PhD thesis, CMM, Ecole des Mines de Paris, 2002.

[9] Allan Hanbury and Jean Serra. Morphological operators on the unit circle. *IEEE Transactions on Image Processing*, 10(12):1842–1850, December 2001.

[10] W. G. Kropatch and H. Macho. Finding the structure of connected components using dual irregular pyramids. In *Cinquiéme Colloque DGCI*, pages 147–158. LLAIC1, Université d'Auvergne, September 1995.

[11] Stéphane Mallat. *A Wavelet Tour of Signal Processing*. Academic Press, 1998.

[12] Fernand Meyer. Graph based morphological segmentation. In *Proceedings of the second IAPR-TC-15 Workshop on Graph-based Representations*, pages 51–60, 1999.

[13] A. Ravishankar Rao. *A Taxonomy for Texture Description and Identification*. Springer-Verlag, 1990.

[14] J. Serra. *Image Analysis and Mathematical Morphology*. Academic Press, London, 1982.

[15] Pierre Soille. *Morphologische Bildverarbeitung. Grundlagen, Methoden, Anwendung*. Springer-Verlag, 1998.